

A Deep Unsupervised Feature Learning Spiking Neural Network with Binarized Classification Layers for the EMNIST Classification

Ruthvik Vaila, *Student Member, IEEE*, John Chiasson, *Fellow, IEEE*, and Vishal Saxena, *Member, IEEE*

Abstract—End user AI is trained on large server farms with data collected from the users. With ever increasing demand for IOT devices, there is a need for deep learning approaches that can be implemented (at the edge) in an energy efficient manner. In this work we approach this using spiking neural networks. The unsupervised learning technique of spike timing dependent plasticity (STDP) and binary activations are used to extract features from spiking input data. Gradient descent (backpropagation) is used only on the output layer to perform the training for classification. The accuracies obtained for the balanced EMNIST data set compare favorably with other approaches. The effect of stochastic gradient descent (SGD) approximations on learning capabilities of our network are also explored. We also introduce SPYKEFLOW, a PYTHON based software tool that we developed.

Index Terms—STDP, Spiking Networks, Surrogate Gradients, EMNIST, Binary Activations, SPYKEFLOW.

I. INTRODUCTION

BIOLOGICAL neurons communicate with each other by transmitting spikes which are $70mV$ voltage pulses while artificial neural networks (ANNs) communicate with each other using floating point computations. There are two popular theories pertaining to how the information is encoded in the spiking input image: rate coding and latency coding. Rate coding stipulates that the information transfer from the input image to the next (hidden) layer is embedded in the rate of spikes coming out of the input neurons. In this work latency coding is used and it refers to the information in the image being encoded in the relative spike times [1] [2]. According to latency coding, earlier spikes (in time) carry more information than later (in time) spikes [1]. The synapses (weights) between spiking neurons are modified according to spike timing dependent plasticity (STDP), where the synapse is strengthened if an input neuron aides the output neuron in spiking (arrives before the output neuron spikes) while the synapse is weakened if an input neuron does not aide the output neurons in spiking (arrives after the output neuron spikes) [3] [4]. As STDP is an unsupervised learning rule, SNNs can be trained layer by layer. The synapses (weights) in ANNs are modified using gradient descent (backpropagation) to reduce the loss defined as an appropriate cost function on the last (output) layer [5]. More specifically, gradient descent is used to update the weights of the network to an acceptable

local minimum of the cost on the output layer [6]. In ANNs input data is fed forward through the network and then the gradient of the cost error is computed layer by layer going backwards to update the weights in each layer. That is, the weights cannot be updated as one feed forwards the input data giving rise to update locking problem [7]. This makes backpropagation a global update rule unlike STDP which is a local update rule [8]. Further, backpropagation uses the same weights for the forward as well as the backward steps, which is referred to as the weight transport problem [9] [10] [11]. Random backpropagation (feedback alignment) was shown to mitigate this problem [12]. A neuromorphic variant of the feedback alignment (random backpropagation) was proposed in [13] and was shown to achieve an accuracy of approximately 98% on the MNIST dataset. Binary neural networks are simply ANNs with binary weights and activations and have been shown to achieve near state-of-the-art classification results with the MNIST [14] and CIFAR-10 [15] datasets. Activations are binarized according to a deterministic or stochastic binarization function, and as binary activations are not differentiable, so called straight through estimators (STE) are used [16] for backpropagation. Panda et al. [17] reported a reduction in energy consumption by a factor of 25 for CIFAR-10 and reduction by a factor of 2 for the IMAGENET dataset [18] by combining existing techniques in deep learning with rate encoded spiking networks. Other works like [19] [20] [21] [22] approximate backpropagation with rate coding and have achieved approximately 98% accuracy on the MNIST dataset. Apart from training spiking networks directly either with supervised or unsupervised methods, alternate methods that convert an existing ANNs to SNNs using transfer learning was introduced by [23]. Masquelier et al. [24] proposed that the earliest spike(s) are sufficient for rapid object classification. The authors in [25] [26] [27] [28] proposed an algorithm to learn exact spike times of temporal coding (latency coding) with gradient descent (backpropagation) on an output cost function. In their approach, activations in ANNs are replaced with spike times and the loss is obtained by calculating the time difference between the desired spike times and the actual spike times. In latency coding minimizing a spike time is conceptually similar to maximizing the activation of a target neuron.

The current literature on spiking networks indicate they give a lower accuracy for classification [29] while standard ANNs employing SGD (floating point computations) are energy inefficient due to the implementation of the algorithms

R. Vaila is a PhD candidate at Department of Electrical and Computer Engineering, Boise State University, Boise, ID, 83706 USA e-mail: ruthvikvaila@u.boisestate.edu

J. Chiasson is with Boise State University, johnchiasson@boisestate.edu.

V. Saxena is with University of Delaware, vsaxena@udel.edu.

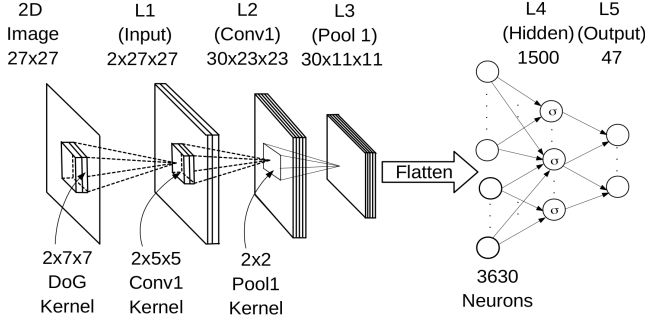


Fig. 1. Layers $L1 - L3$ are the feature extraction layers and layer $L3 - L5$ are the feature classification layers.

on high precision computers. Energy-efficiency (low power consumption) and state-of-the-art classification accuracy are important goals. In this paper, we approach this by combining STDP and approximate SGD with binary activations to achieve near state-of-the-art classification accuracy on EMNIST and MNIST datasets.

II. NETWORK DESCRIPTION

Our network is shown in Figure 1. The extraction layers of this network is similar to that of [30] [31].

A. Input Encoding

Following [30] [31], K_{σ_1, σ_2} is a Difference of Gaussian (DoG) filter with $\sigma_1 = 1, \sigma_2 = 2$ for the ON-center and $\sigma_1 = 2, \sigma_2 = 1$ for the OFF-center, given by

$$K_{\sigma_1, \sigma_2}(i, j) = \begin{cases} \frac{1}{2\pi\sigma_1^2} e^{-\frac{i^2 + j^2}{2\sigma_1^2}} - \frac{1}{2\pi\sigma_2^2} e^{-\frac{i^2 + j^2}{2\sigma_2^2}} & \text{for } -3 \leq i, j \leq 3 \\ 0, & \text{otherwise} \end{cases} \quad (1)$$

Plots of ON and OFF center filters are shown in Figure 2. The input image is convolved with ON and OFF centered filters, resulting in two “images” which are then converted to an ON and an OFF spiking image.

$$\Gamma_{\sigma_1, \sigma_2}(u, v) = \sum_{j=-3}^{j=3} \sum_{i=-3}^{i=3} \mathbf{I}_{in}(u+i, v+j) K_{\sigma_1, \sigma_2}(i, j) \quad (2)$$

for $0 \leq u \leq 26, 0 \leq v \leq 26$.

At each location (u, v) of the output image $\Gamma_{\sigma_1, \sigma_2}(u, v)$ a unit spike $s_{(u, v)}$ is produced if and only if $\Gamma_{\sigma_1, \sigma_2}(u, v)$ exceeds a threshold i.e.,

$$\Gamma_{\sigma_1, \sigma_2}(u, v) > \gamma_{DoG} \quad (3)$$

where $\gamma_{DoG} = 50$ was chosen [32]. The spike times are encoded relatively depending on magnitude of the membrane potentials and the relation is given by

$$\tau_{(u, v)} = \frac{1}{\Gamma_{\sigma_1, \sigma_2}(u, v)} \text{ in milliseconds.}$$

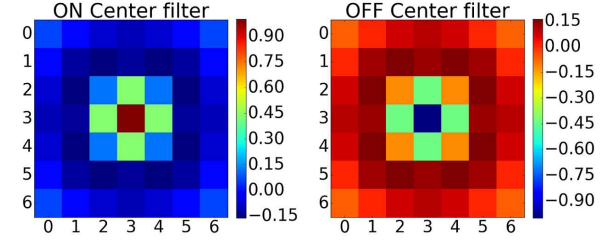


Fig. 2. ON center filter has higher values at the center whereas OFF center filter has lower values at the center. Colour code indicates the filter values.

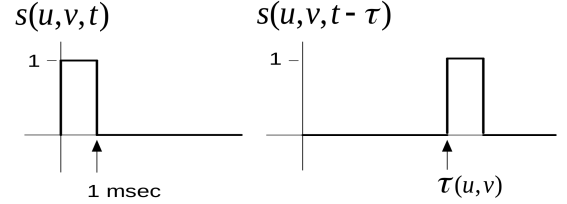


Fig. 3. Left: Spike signal from the input image with no time delay. Right: Spike signal from the input image with a delay of τ milliseconds.

The spike signal $s_{(u, v)}(t)$ is latency (temporally) encoded [1] by delaying it by an amount inversely proportional to $\Gamma_{\sigma_1, \sigma_2}(u, v)$ as shown in Figure 3. That is, the greater the value of $\Gamma_{\sigma_1, \sigma_2}(u, v)$, the sooner the neurons spikes and vice versa. Equivalently, the value of $\Gamma_{\sigma_1, \sigma_2}(u, v)$ is encoded in the value $\tau_{(u, v)}$. Note that a neuron at location (u, v) can generate at most one spike. Silicon retinas such as eDVS [33] directly provide spiking images. The authors used such images in [34] [35].

B. Convolution Layers and STDP

We denote a spike at time t emanating from the (u, v) neuron of a spiking image by $S_{L1}(t, k, u, v)$, where $k = 0$ (ON center) or $k = 1$ (OFF center) and $(0, 0) \leq (u, v) \leq (27, 27)$. Layer $L2$ (Conv1) consists of 30 (feature) maps with each map having its own convolution kernel given by

$$W_{C1}(w, k, i, j) \in \mathbb{R}^{30 \times 2 \times 5 \times 5} \text{ for } w = 0, 1, 2, \dots, 29$$

The instantaneous “membrane potential” of the (u, v) neuron of a feature map w ($w = 0, 1, 2, \dots, 29$) of layer $L2$ (Conv1) at time t is given by

$$V_{L2}(t, w, u, v) = \sum_{t=0}^{\tau} \left(\sum_{k=0}^1 \sum_{i=0}^4 \sum_{j=0}^4 S_{L1}(t, k, u+i, v+j) W_{C1}(w, k, i, j) \right) \quad (4)$$

for $0 \leq (u, v) \leq 22$

If at time t the membrane potential of a neuron in a feature map w at location (u, v) crosses a set threshold value

$$V_{L2}(t, w, u, v) > \gamma_{L2} = 15$$

then the neuron at (w, u, v) produces a spike at time t .

At any time t , all of the potentials $V_{L2}(t, w, u, v)$ for $(0, 0) \leq (u, v) \leq (22, 22)$ and $w = 0, 1, 2, \dots, 29$ are computed in parallel. Neurons in different locations within a map and in different maps may have spiked. In particular, at the location

(u, v) there can be multiple spikes (up to 30) produced by 30 different neuron belonging to 30 different maps. The desire is to have different maps learn different features so that all the important features in the input image can be captured. To enforce this condition, *lateral inhibition* and *STDP competition* are used [30].

1) *Lateral Inhibition*: To explain lateral inhibition suppose at the location (u, v) there were potentials $V_{L2}(t, w, u, v)$ in different maps (w goes from 0 to 29) at time t that exceeded the threshold γ_{L2} . Then the neuron in a map with the highest potential $V_{L2}(t, w, u, v)$ at (u, v) inhibits the neurons in all the other maps at the location (u, v) from spiking for the current image (even if the potentials in the other maps exceeded the threshold). Figure 4 (left) shows the accumulated spikes (from an MNIST image of “5”) for 12 time steps from all 30 maps of Layer $L2$ at each location (u, v) *without* lateral inhibition. For example, at location (19,14) in Figure 4 (left) the color code is yellow indicating in excess of 20 spikes, i.e., more than 20 of the maps produced a spike at that location.

Figure 4 (center) shows the accumulation of spikes from all 30 maps for 12 time steps, but now *with* lateral inhibition imposed. Note that at each location there is at most one spike indicated by the color code. Also, as explained next, only a few of these spikes will actually result in the update of any of the 30 kernels (weights) of layer $L2$.

2) *STDP Competition*: After lateral inhibition we consider each of the maps in layer $L2$ that had one or more neurons with their potential V exceeding γ . Let these maps be $w_{k1}, w_{k2}, \dots, w_{km}$ where¹ $0 \leq k_1 < k_2 < \dots < k_m \leq 29$. Then in each map w_{ki} we locate the neuron in that map that has the maximum potential value. Let

$$(u_{k1}, v_{k1}), (u_{k2}, v_{k2}), \dots, (u_{km}, v_{km}) \quad (5)$$

be the location of these maximum potential neurons in each map. Then neuron (u_{ki}, v_{ki}) inhibits all other neurons in its map w_{ki} from spiking for the remainder of the time steps of the current spiking image. Further, these m neurons can inhibit each other depending on their relative location as we now explain. Suppose neuron (u_{ki}, v_{ki}) of map w_{ki} has the highest potential of the m neurons in (5). Then, in an 11×11 area centered about (u_{ki}, v_{ki}) , this neuron inhibits all neurons of all the other maps in the same 11×11 area. Next, suppose neuron (u_{kj}, v_{kj}) of map w_{kj} has the second highest potential of the remaining $m - 1$ neurons. If the location (u_{kj}, v_{kj}) of this neuron was within the 11×11 area centered on neuron (u_{ki}, v_{ki}) of map w_{ki} , then it is inhibited. Otherwise, this neuron at (u_{kj}, v_{kj}) inhibits all neurons of all the other maps in a 11×11 area centered on it. This process is continued for the remaining $m - 2$ neurons. In summary, there can be no more than one neuron that spikes in the same 11×11 area of all the maps.² The right side of Figure 4 shows the final winner spike accumulation for 12 time steps across 30 maps after both lateral inhibition and STDP competition have been imposed. It also shows that there is at most one winner spike from all

the maps in any 11×11 area. For this particular input image (the number 5), these five winner spikes are from maps 14, 16, 19, 21, and 23 at locations (19, 4), (3,10), (17, 15), (9,12) and (3,19), respectively and will result in updates for these 5 map kernels (weights). Lateral inhibition STDP competition resulted in an average of only 5.8 spikes per image from the $30 \times 22 \times 22$ neurons in $L2$ during training with EMNIST dataset. Figure 5 shows how the randomly initialized weights evolved for all 30 maps after training with 6000 images.

3) *Spike Feature Vectors* : After (unsupervised) training of the weights (synapses) in the $L2$ layer, these weights are fixed. Spike feature vectors are created by passing spiking input images through layer $L2$ (Conv1) *with lateral inhibition enforced* and *without STDP competition* as there is no training involved. The spikes coming out of the $L2$ layer are then pooled in the $L3$ layer *without lateral inhibition*. The pooling is done on an area of 2×2 neurons in $L2$ with a stride of 2. Specifically, in each 2×2 area of $L2$ which contains 4 neurons, the spike of the neuron with the maximum membrane potential V_{L2} , assuming it exceeds the threshold γ_{L2} , is then the spike of the corresponding neuron of the $L3$ (pooling) layer (i.e., thresholding on maxpooling). For the EMNIST dataset each input image results in a spike tensor of shape $\tau \times 30 \times 11 \times 11$. We set τ to be 12 and these tensors were summed across it's first axis (i.e, along time). The resulting tensors in $R^{30 \times 11 \times 11}$ were flattened.³

Once a neuron in $L3$ spikes, it is not allowed to spike again for the rest of the time steps in the current image. This results in the spike feature vectors being *binary* valued (i.e., vectors of zeros and ones). In our experiments an average of 125 spikes/image come out of $L3$ from the $30 \times 11 \times 11 = 3630$ neurons for the EMNIST dataset. As the activations of $L4$ are *binary* (non differentiable), in order to do the backpropagation from layer $L5$ back to layer $L3$ a *surrogate* gradient is used (see Section IV below).

4) *Weight Initialization* : The weights of the $L2$ layer are initialized from the normal distribution $\mathcal{N}(0.8, 0.04)$. The weights of layers $L4$ & $L5$ layers are initialized from the normal distribution $\mathcal{N}(0, 0.01)$, but truncated to keep them between ± 0.02 . A softmax activation is used for the classification layer $L5$ with its (net) inputs converted to integers using the floor function. A table of values of the exponential function e^x can be stored in a look-up table so that the softmax activation can be calculated using this lookup table in a hardware implementation. The activations functions in layer $L4$ (denoted σ in Figure 1) are discussed below (see Section IV below).

C. Spike Timing Dependent Plasticity (STDP)

Spike timing dependent plasticity defines how a synapse (weight) between an input (pre-synaptic) neuron and an output (post-synaptic) neuron is modulated (updated). In its simplest form [30], STDP strengthens the synapse (weight) between an input and output neuron if the input neuron aids the output

¹The other maps did not have any neurons whose membrane potential crossed the threshold and therefore cannot spike.

²The use of the number 11 for the 11×11 inhibition area of neurons was suggested by Dr. Kheradpisheh [32].

³If more convolution layers are desired, spike tensors collected in $L3$ layer can be used for unsupervised training of any subsequent convolutional layers.

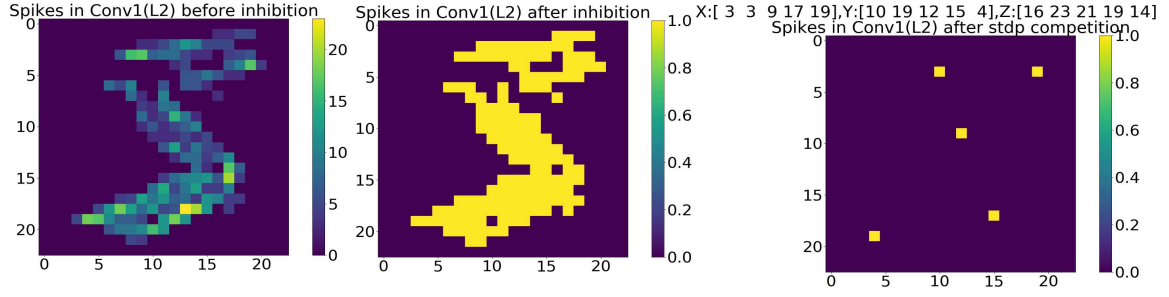


Fig. 4. Left: EMNIST digit "5" input. Accumulation of spikes from all 30 maps and 12 time steps in L2 *without* lateral inhibition. Center: Accumulation of spikes from all 30 maps and all 12 time steps in L2 *with* lateral inhibition. Right: Accumulation of spikes across all maps and 12 time steps with both lateral inhibition and STDP competition imposed for a single image. X, Y denote the location of neuron in a map and Z denotes the map number. Note that these five winner spikes suppress all the other neurons that crossed the threshold.

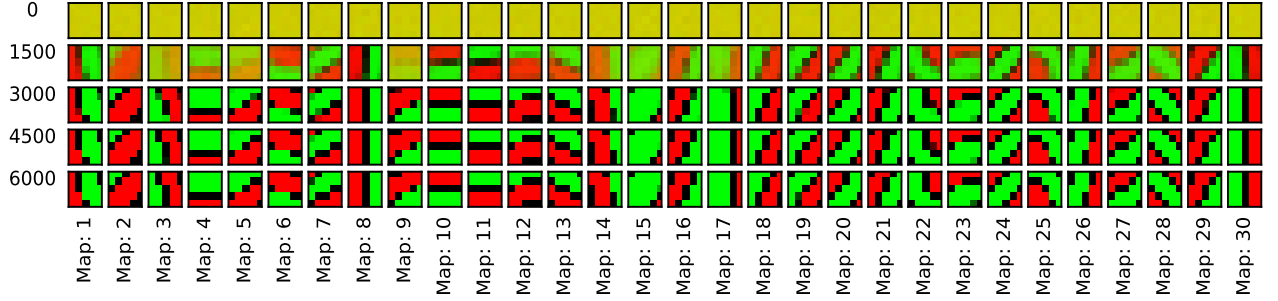


Fig. 5. Evolution of learning in the first convolution layer. Red and Green indicate ON and OFF center synapses respectively.

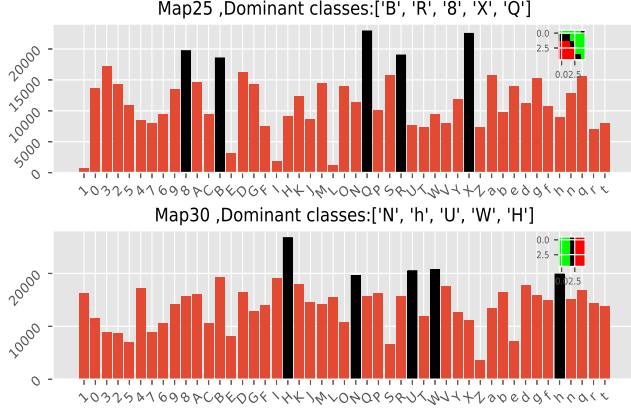


Fig. 6. Spikes per map per label in L3 (Pool 1). Highlighted (in black) are the classes that resulted in most number of spikes in a particular feature map. Feature learned by the corresponding map is shown in the inset.

neuron in overcoming the membrane threshold (spiking); otherwise the synapses are weakened. With t_{out} and t_{in} denoting the spike time of the output (post-synaptic) and the input (pre-synaptic) neuron, respectively, the STDP learning rule used here is given by

$$\Delta w_i = \begin{cases} -a^- w_i (1 - w_i), & \text{if } t_{out} - t_{in} < 0 \\ +a^+ w_i (1 - w_i), & \text{if } t_{out} - t_{in} \geq 0 \end{cases} \quad (6)$$

$$w_i \leftarrow w_i + \Delta w_i$$

Learning in spiking networks refers to the change Δw_i in the (synaptic) weight. The learning rate parameters a^+ and

a^- are initialized with low values (0.004, 0.003) [30] [31] and are typically increased as the learning progresses. In our experiments we doubled the learning rate for every 1500 input images. As there are neither labels nor a cost function involved in the process of STDP, it is an *unsupervised* learning algorithm. That is, the weights can be updated during the feed forward step in SNNs. In contrast, ANNs update their weights during error the feed back step. So, STDP does not suffer from the update locking phenomenon [7]. Synapses in feature extraction section of the network in Figure 1 were updated at the end of every time step.

III. BACKPROPAGATION IN THE L3-L5 LAYERS

Stochastic gradient descent (SGD) via backpropagation is the primary choice for state-of-the-art classification, regression, and generative learning. A cost function is assigned to the last layer of the network and the synapses are updated to minimize the cost. In our network, backpropagation is used only in the classification layers (L3-L4-L5) of the network which has a single hidden layer L4. Let $\delta^l, a^l (= \sigma(z^l)), b^l, W^l, z^l (= w^l z^{l-1} + b^l)$ denote the error vector, the activation vector, the bias vector, the weights and the net input to the activation function for the l^{th} layer, respectively [36]. σ is the activation function. With C denoting the output cost, the backpropagation equations are

$$\delta^L = \nabla_a C \odot \sigma'(z^L) \quad (7)$$

where δ^L denotes the error vector on the last layer and the error vector for the hidden layers is given by

$$\delta^l = ((W^{l+1})^T \delta^{l+1}) \odot \sigma'(z^l) \quad (8)$$

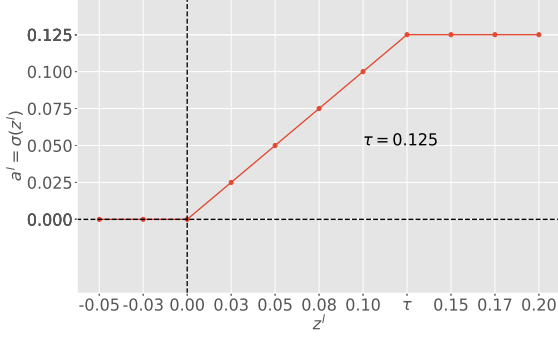


Fig. 7. Activation function $a^l = \sigma(z^l)$ for neurons in layer $L4$.

Updates to biases and weights of layer l are calculated with

$$\frac{\partial C}{\partial b^l} = \delta^l \quad (9)$$

$$\frac{\partial C}{\partial W^l} = \delta^l a^{(l-1)T} \quad (10)$$

C denotes the cost in the final layer. We used a softmax activation with a cross entropy cost function for the last layer so that equation (7) becomes

$$\delta^L = -(y - a^L), \quad (11)$$

where a^L and y are softmax activation of the output layer and the one hot label vector, respectively.

IV. SURROGATE FOR THE GRADIENT

The output activation function of $L3, L4$ layers is discontinuous and consequently it does not have a derivative. Here we give two different possible functions that we used to take the place of the gradient, i.e., be its surrogate [16].

A. Surrogate Gradient 1

The activation function of a neuron in layer $L4$ is defined by

$$a^l = \sigma(z^l) \triangleq \begin{cases} 0, & z < 0 \\ z, & 0 \leq z < \tau \leq 1 \\ \tau, & z \geq \tau. \end{cases} \quad (12)$$

Figure 7 is a plot of this activation function which is a ReLU that saturates at $\tau \leq 1$.

The activation activation is required to be binary so its definition is modified to be ($\lceil \cdot \rceil$ denotes the ceiling function)

$$a^l = \lceil \sigma(z^l) \rceil \triangleq \begin{cases} 1, & z \geq 0 \\ 0, & z < 0 \end{cases} \quad (13)$$

For this activation (13) we define its surrogate gradient to be

$$\sigma'(z^l) \triangleq \begin{cases} 1, & 0 \leq z < \tau \leq 1 \\ 0, & \text{otherwise.} \end{cases} \quad (14)$$

which is the derivative of Equation 12.

Simulations were performed by setting τ to 0.25, 0.125, 0.05 and we found that 0.125 maximizes

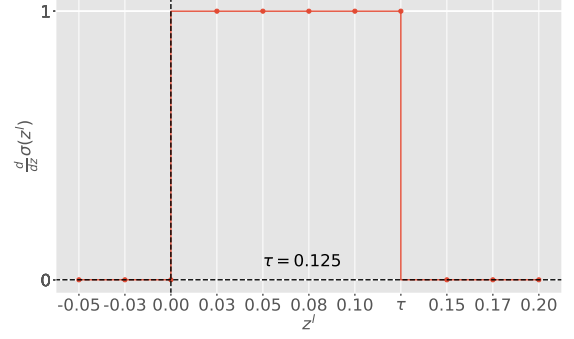


Fig. 8. Surrogate gradient of activation function defined in equation (12).

the validation accuracy. Since error backpropagation is not feasible with equation (13), we take derivative of $\sigma(z)$ to be equation (14). For convenience, we denote an activation value of 1 as spike and an activation value of 0 as no spike.

B. Surrogate Gradient 2

We also considered a second activation given by

$$a^l = \sigma(z^l) \triangleq \begin{cases} 1, & z \geq 0 \\ 0, & z < 0 \end{cases} \quad (15)$$

and define its surrogate gradient to be

$$\sigma'(z^l) \triangleq \begin{cases} 1, & z \geq 0 \\ 0, & z < 0 \end{cases} \quad (16)$$

Note that $\sigma'(z) = \sigma(z)$ and is binary so that $a^l = \sigma'(z^l)$ in the hidden layer. Equation (8) then becomes

$$\delta^l = ((W^{l+1})^T \delta^{l+1}) \odot a^l \quad (17)$$

where a^l determines if a neuron spikes in the l^{th} layer. Hence a^l determines if a neuron in the l^{th} layer is to receive error information from the $l+1$ layer. Substituting Equation (17) in Equation (10) gives

$$\frac{\partial C}{\partial W^l} = ((w^{l+1})^T \delta^{l+1} \odot a^l) a^{(l-1)T} \quad (18)$$

We see that a neuron in $l-1$ layer gets to update its synapse with a neuron in l^{th} layer if both neurons have spiked, i.e., for $\partial C / \partial W_{pq}^l$ to be a non-zero both a_p^l and a_q^{l-1} have to be non-zero.

V. MNIST

Our interest here is the EMNIST dataset. However, as the MNIST handwritten digits dataset is a popular benchmark, we briefly present our results with it [14]. The MNIST digits were passed through the network in Figure 1 and encoded into spike vectors (described in Section II-B3). Note that the extracted features are *binary* valued. Table I shows that surrogate gradient 1 yields a test accuracy 0.74% higher or 74 more correct classifications compared to surrogate gradient 2 with 10,000 test images. Figure 9 shows the classification accuracy per class using the surrogate gradient 1.

TABLE I

CLASSIFICATION ACCURACIES ON THE MNIST DATASET. DROPOUT (50%) MECHANISM WAS USED IN HIDDEN LAYER FOR REGULARIZATION AND NUMBER OF NEURONS IN LAYER L4 WERE SET TO 900. THESE RESULTS WERE OBTAINED BY AVERAGING OVER FIVE EXPERIMENTS WITH THE CLASSIFICATION LAYERS OF THE NETWORK (IN FIGURE 1) TRAINED FOR 30 EPOCHS EACH TIME. FOR ACCURACIES REPORTED USING THE ACTUAL GRADIENT A QUADRATIC COST FUNCTION WITH A ReLU ACTIVATION FUNCTION FOR LAYERS L4, L5 WAS USED WHEREAS FOR ACCURACIES REPORTED USING THE SURROGATE GRADIENTS A CROSS-ENTROPY COST FUNCTION WITH SOFTMAX APPROXIMATION (SEE SECTION II-B4) FOR LAYER L5 AND BINARY ACTIVATION FUNCTION FOR LAYERS L3, L4 WAS USED. MINI BATCH SIZE WAS SET TO 5. η FOR THE ACTUAL AND SURROGATE GRADIENTS WAS SET TO 0.0125 AND 0.01, RESPECTIVELY.

Gradient Type	Mean Test Acc.	Max. Test Acc.
Actual Gradient	98.58%	98.66%
Surrogate Gradient 1	98.49%	98.54%
Surrogate Gradient 2	97.75%	97.77%

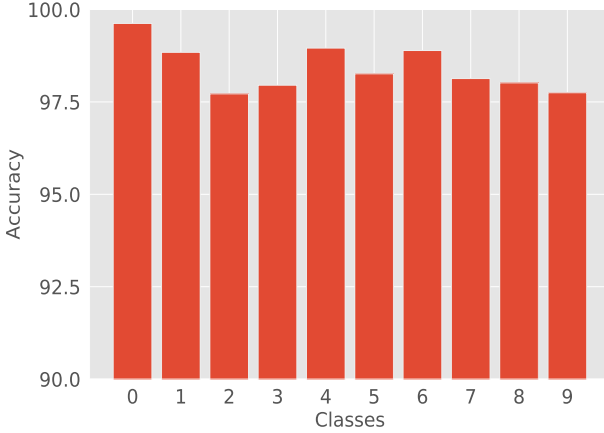


Fig. 9. Classification accuracy per class of MNIST dataset with surrogate gradient 1.

VI. EMNIST

EMNIST dataset has 47 classes containing handwritten upper & lower case letters of the English alphabet in addition to the digits. This dataset is divided into 102,648 training images, 10,151 validation images, and 18,800 test images [37].

A. Backpropagation with Gradient

The features were extracted in an unsupervised fashion in layers L1, L2, and L3 of the network (Figure 1). As described in Section II-B3 the neurons in L3 can spike no more than once for an image resulting in *binary* valued spike feature vectors (i.e., vectors of 0s and 1s). These extracted *binary* valued spike feature vectors were classified using an ANN with a ReLU activation for the hidden layer L4 neurons and a softmax output activation function. The classification accuracies on EMNIST dataset are given in Table II.

Figure 10 shows 60 examples of misclassified classes. About 2688 (14.3%) of 18800 test images were misclassified. On further examination we found that classes {f,F}, {0,O} the digit “0” and upper case “O”, {q,q} lower case “q” and

TABLE II

CLASSIFICATION ACCURACIES ON EMNIST DATASET. DROPOUT OF 50% WAS USED IN THE HIDDEN LAYER AND THE NUMBER OF NEURONS IN LAYER L4 WAS 1500. THESE RESULTS WERE OBTAINED BY AVERAGING OVER FIVE EXPERIMENTS AND TRAINED FOR 25 EPOCHS EACH TIME.

Gradient Type	Mean Test Acc.	Max Test Acc.	η	Activation
Actual Gradient	85.47%	85.7%	0.05	ReLU

the digit “9”, {1, l, L} the digit “1”, upper case “I” (eye) and upper case “L”, {S,5} upper case “S” and the digit “5”, {2,Z} the digit “2” and upper case “Z” were frequently misclassified. For example, in the upper left corner of Figure 10 the network predicted a lower case “f” while the label was an upper case “F”. Figure 12 shows the confusion matrix for the classified data. For example, the digit “0” was mistaken to be an upper case “O” frequently. Similarly, upper case “I” was often mistaken to be an upper case “L”.

1) Conditioning on Upper Case, Lower Case and Digits:

With handwritten data, even a human classifier may not be able to tell the difference between, for example, the upper case letter “O” and the digit “0”. To study this we also ran the classifier conditioned on (given that) the image under test was an either an upper case letter, a lower case letter or a digit. No retraining was done for this section. Table III shows the dramatic increase in accuracy from 85.6% to 94.49% when using this conditioning. The accuracy per class using this conditioning is given in Figure 14. It is seen that the classes I, L, g, q have the least recognition rate, but still well above their accuracies given previously in Figure 11 where conditioning was not used. In more detail we found that about 11% of the letters “q” were misclassified as the letter “g”, about 4% of letters “q” were misclassified as the letter “a”, while about 84% of letters “q” were correctly classified. About 26% of letters “g” were misclassified as the letter “q” while about 67% of letters “g” were correctly classified. Similarly, we found that about 22% of letters of upper case “I” (eye) were misclassified as the upper case letter “L” while 73% of upper case “I” were correctly classified. As a final observation about 22% of upper case letters “L” were misclassified as an upper case “I” (eye) while about 76% of upper case letters “L” were correctly classified.

TABLE III

CLASSIFICATION ACCURACIES ON EMNIST DATASET CONDITIONED ON INPUT BEING A DIGIT, UPPER CASE OR A LOWER CASE LETTER.

Conditioned Maximum Test Accuracy
94.49 %

B. Backpropagation with Gradient Surrogates

In this section *binary* valued features vectors (i.e., vector with 0s and 1s) were collected in layer L3 as described in Section II-B3. Classification was performed using an ANN with binary activation for the hidden layer L4 neurons and an approximated softmax output explained in Section II-B4. Table IV shows that the gradient surrogate 1 outperforms gradient surrogate 2 by 1.0% (188 more correct classifications with 18800 test images).

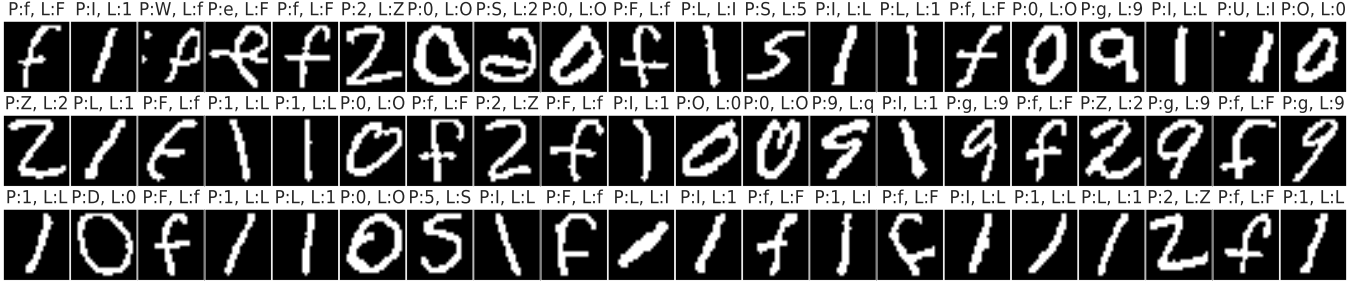


Fig. 10. Frequently misclassified classes in the EMNIST dataset. P and L denote predicted class and actual label, respectively.

TABLE IV

CLASSIFICATION ACCURACIES ON EMNIST DATASET. DROPOUT (50%) MECHANISM WAS USED IN HIDDEN LAYER FOR REGULARIZATION AND NUMBER OF NEURONS IN L4 WAS SET TO 1500. A CROSS ENTROPY COST FUNCTION WITH SOFTMAX APPROXIMATION (SEE SECTION II-B4) WAS USED. THESE RESULTS WERE OBTAINED BY AVERAGING OVER FIVE EXPERIMENTS WITH THE CLASSIFICATION LAYERS OF THE NETWORK (IN FIGURE 1) TRAINED FOR 25 EPOCHS EACH TIME. BATCH SIZE WAS SET TO 5.

Gradient Type	Mean Test Acc.	Max. Test Acc.	Conditioned Max. Test Acc.	η	Activation
Surrogate Gradient 1	85.35 %	85.49 %	94.1 %	0.02	Binary
Surrogate Gradient 2	84.24 %	84.47 %	93.72 %	0.02	Binary

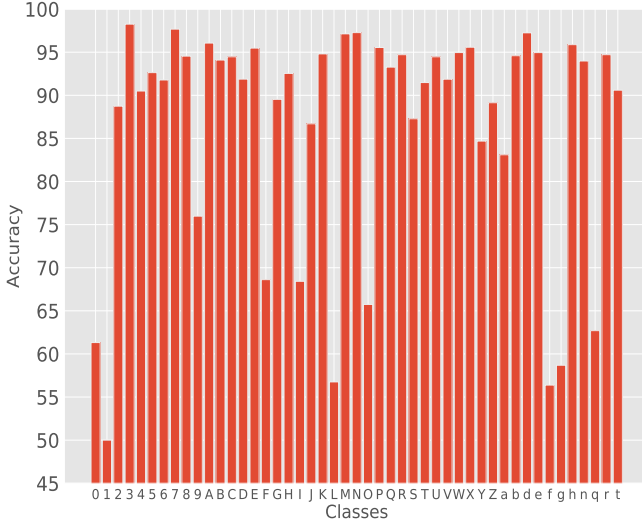


Fig. 11. Accuracy per class of EMNIST dataset. For example, only about 61% of digits “0” were classified correctly as many of them were misclassified as the letter “O”.

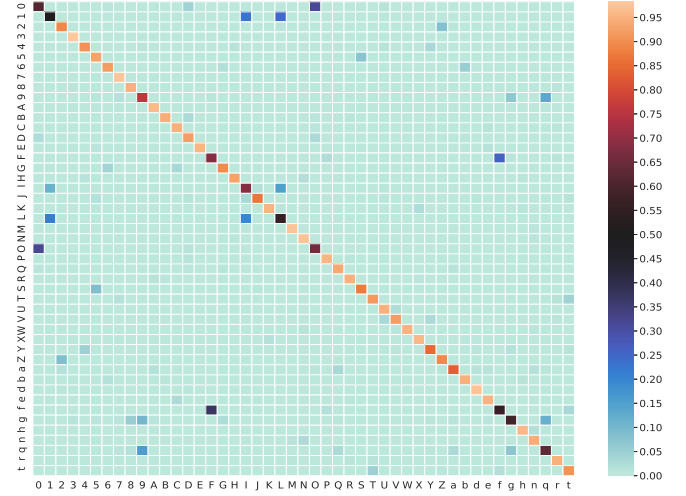


Fig. 12. Confusion matrix of predictions with EMNIST dataset.

a) Computational Advantage of Binary Activations:

In the feedforward paths L1 through L4 the matrix-vector multiplication operations can all be avoided in a hardware implementation as these layers all have binary activations. For example, executing the multiplication of a set of (floating point) weights times a set of spikes (binary activations) is simply

$$\begin{pmatrix} W_{11} & W_{12} & W_{13} \\ W_{21} & W_{22} & W_{23} \\ W_{31} & W_{32} & W_{33} \\ \vdots & \vdots & \vdots \\ W_{n1} & W_{n2} & W_{n3} \end{pmatrix} \times \begin{pmatrix} 0 \\ 1 \\ 1 \end{pmatrix} = \begin{pmatrix} W_{12} \\ W_{22} \\ W_{32} \\ \vdots \\ W_{n2} \end{pmatrix} + \begin{pmatrix} W_{13} \\ W_{23} \\ W_{33} \\ \vdots \\ W_{n3} \end{pmatrix}. \quad (19)$$

That is, multiplication is replaced by addition. This technique avoids the need for dedicated multiplier hardware and allows

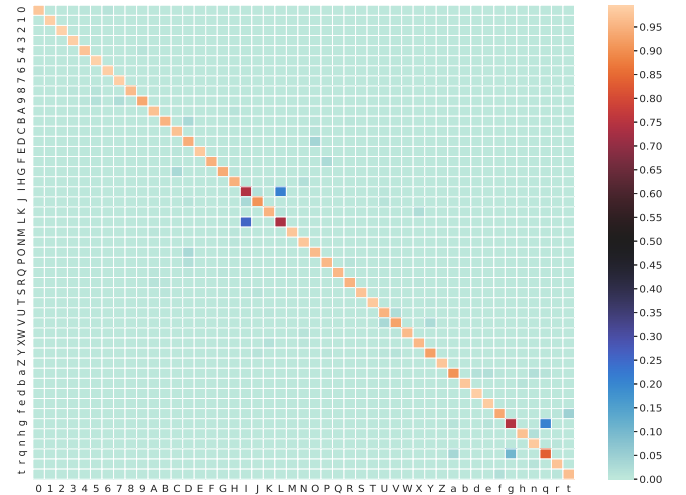


Fig. 13. Confusion matrix of classification with EMNIST dataset after the input was conditioned on being a digit, upper case or a lower case letter.

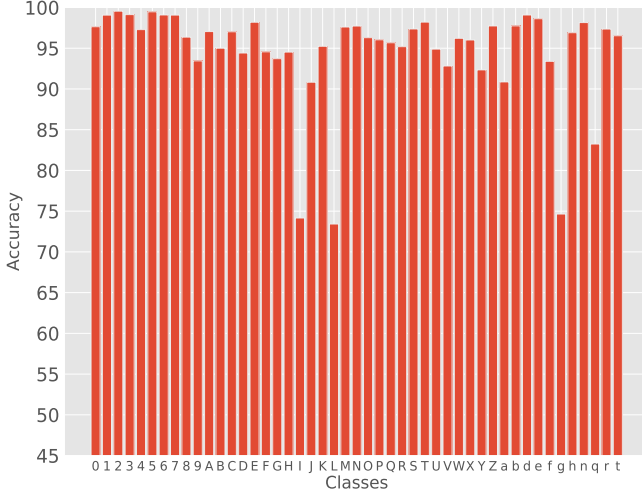


Fig. 14. Accuracy per class after conditioning.

the feasibility of in memory computing [38] [39]

Another advantage is found in backpropagation computations. Specifically, as the surrogate gradient $\sigma'(z^l)$ is binary, the error vector δ^l for the hidden layer can be obtained without having to do some of the row-column multiplications in

$$((W^{l+1})^T \delta^{l+1}) \odot \sigma'(z^l).$$

For example

$$\underbrace{\begin{pmatrix} w_{11} & w_{12} \\ w_{21} & w_{22} \end{pmatrix}}_{(w^{l+1})^T} \times \underbrace{\begin{pmatrix} 1 \\ 2.5 \end{pmatrix}}_{\delta^{l+1}} \odot \underbrace{\begin{pmatrix} 0 \\ 1 \end{pmatrix}}_{\sigma'(z^l)} = \begin{pmatrix} 0 \\ w_{21} + 2.5w_{22} \end{pmatrix} \quad (20)$$

That is, in equation (20) the row-column multiplications of the first row are avoided as the result will be zero due to the element-wise (Hadamard product) vector multiplication. All the weight updates, $\partial C / \partial W^l$ can be obtained without explicitly calculating vector outer product $\delta^l a^{(l-1)T}$ as the activations of $L3$ and $L4$ layers are binarized. For example

$$\underbrace{\begin{pmatrix} a \\ b \\ c \end{pmatrix}}_{\delta^l} \times \underbrace{\begin{pmatrix} 0 & 1 & 0 \end{pmatrix}}_{a^{(l-1)T}} = \begin{pmatrix} 0 & a & 0 \\ 0 & b & 0 \\ 0 & c & 0 \end{pmatrix}. \quad (21)$$

That is, the matrix on the right side of Equation (21) is found by simply transcribing δ^l into its columns as specified by $a^{(l-1)T}$.

VII. SOFTWARE TOOL

Previously the authors have used the PYNNS simulator with NEURON [40] [41]. However these are tools for neuroscientists with neuron models much more complex than needed in our case. Even tools like NENGO [42] (developed for bio-inspired machine learning) use more complex neuronal models than necessary here. Motivated by the simple spiking models in Kheradpisheh et al.'s work in [30], we developed our software tools. Following [30] our package supports instantaneous (non leaky integrate and fire) neurons, latency encoding, and

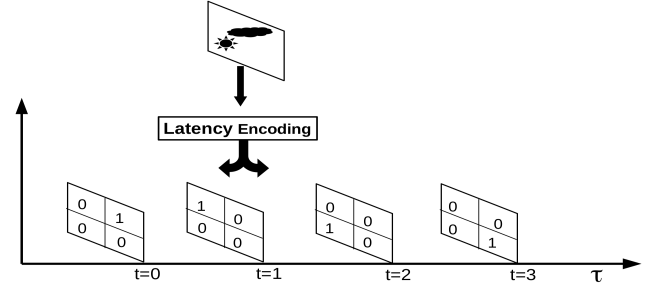


Fig. 15. Spikes are represented with a value 1 and no spike is represented with a value 0. In this figure τ was set to 4.

inhibition mechanisms to be able to simply extract meaningful features from the input images. Feature extraction in SNNs is unsupervised in contrast to ANNs. To monitor the weight updates (synapse changes) in the spiking network, the software provides the capability to monitor spike activity, weight evolution (updates), feature extraction (spikes per map per label), and synapse convergence, etc. This software tool was used here and in [34] [35]. Similar to our work, Mozafari et al released the software tool SPYKETORCH in [43] which is based on the PYTORCH [44] deep learning tool. Our software is named SPYKEFLOW⁴ and primarily uses NUMPY [45] to do the calculations of lateral inhibition, STDP updates, neuron spike accumulation, etc. However, we also use TENSORFLOW [46] for computationally intensive calculations such as convolution and pooling. Therefore, the users will have the ability to use a GPU, if one is available. Visualizations are performed using MATPLOTLIB [47] and we also provide some miscellaneous JUPYTER notebooks. SPYKEFLOW is divided into two main classes: feature extraction and feature classification. Firstly, input images (2D) are converted to tensors of three dimensions with time t as the extra dimension. For example, Figure 15 shows that an input (2D) image converted to a spiking image represented by a rank 3 tensor of binary values. Spikes are arranged into τ slices based on latency encoding described in Section II. Figure 15 also indicates that if an input neuron spikes (binary 1) it is not allowed to spike for the rest of the image. In all of our experiments we set $\tau = 12$ so $t = 0, 1, \dots, 11$. Batch size in our software is 1 time step which means the synapses are updated after every 1 time step. The file structure of SPYKEFLOW is shown below

```
AllDataSets/
spykeflow/
  network.py
  inputlayerclass.py
  classifierclass.py
  .
  .
main/
  main.py
notebooks/
outputs/
```

The AllDataSets folder contains all the datasets that we intend to work with and the folder spykeflow contains

⁴<https://github.com/ruthvik92/SpykeFlow>

core classes of the tool. The main folder contains the main.py file which contains the code to perform feature extraction, visualization, and classification. The notebooks folder contains the JUPYTER notebooks for classification part of the network (in Figure 1) and show the code for various backpropagation approximations that were used in this work. The outputs folder contains plots generated by SPYKEFLOW for various datasets. Contents of main.py file are discussed below

A. Conv1 and Pool 1 layers

```
import numpy as np
import os, sys, random
sys.path.insert(0, "path_to_SpykeFlow")
import spykeflow as sf
os.environ["CUDA_VISIBLE_DEVICES"]="-1"
from spykeflow import network as network
from spykeflow import classifierclass as cls
from spykeflow import inputlayerclass as inputlayer
# Input layer
firstLayer = inputlayer.InputLayer(debug=False,
size=27, dataset=data_set, off_threshold=50,
on_threshold=50, border_size=2, data='test',
val_frac=0.14, test_frac=0.14)
test_input_data=firstLayer.EncodedData()
#returned data is in [(data_tensor1, data_label1),\
#(data_tensor2, data_label2), .....]
random.shuffle(train_input_data)
class_labels_train = map(lambda x: np.where(\
x[1]==1)[1][0], train_input_data)
labels_dict = {0:'0', 1:'1', ..., 45:'r', 46:'t'}
nofImages = 6000
train_input_images = [items[0] for items \
in train_input_data][0:nofImages]
train_input_images = np.concatenate(\
train_input_data, axis=3)
size = train_input_images.shape[0]
T = train_input_images.shape[-1] #Total time steps
#First Conv layer, pool is disabled as train=True
net1 = network.Network(output_channels=30, inputs=\
train_input_images, A_plus=0.002, debug=False,\
sample_interval=200, train=True,\
save_pool_spike_tensor=False, threshold=15.0,\
size=size, inh_reg=11)
#Start training
net1.feedforward()
```

Running `net1.feedforward()` executes the following algorithm.

Method `net1.feedforward()`

```
for t in range(0,T)
    if(t%r==0)#end of current image
        Reset neurons
        Feed forward for 1 timestep
        Lateral inhibition
        STDP competition
        Determine final spikes
        STDP weight updates
        Record weights,spikes
```

If debug is set to True in the object `net1` then a series of images showing the internal activity of the network are shown. Figure 16 and Figure 17 show the steps carried out

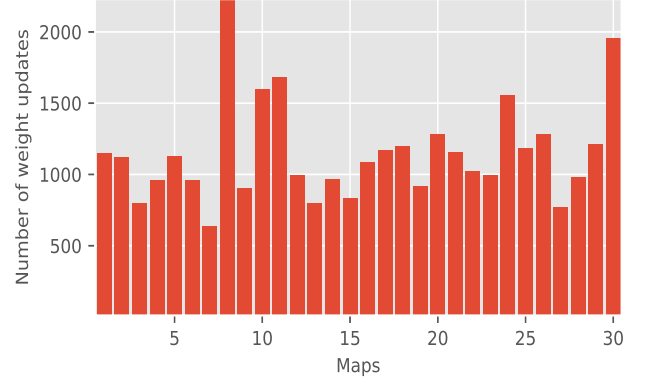


Fig. 18. Number of spikes that resulted in STDP weight updates per map.

in L2 (Conv1) layer to determine the spikes that result in a weight update.

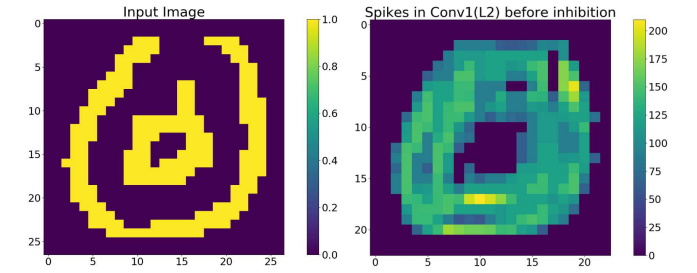


Fig. 16. Left: Input spikes. Right: Neurons in in Conv1 (L2) that crossed the threshold. Number of times a neuron in an X-Y location across all the maps (features) that crossed the threshold is indicated by the color code. Spikes are summed across time and number of maps for visualization.

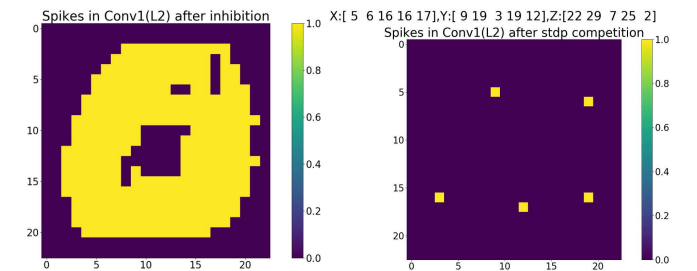


Fig. 17. Left: Neurons that crossed threshold in L2 after lateral inhibition. Right: Final spikes in L2 after STDP competition. Number of neurons that crossed the threshold in an X-Y location is indicated by the color code. Z indicates the map number. Spikes are summed across time and number of maps for visualization.

1) *Generating plots:* Once the training of the first convolutional layer is finished, plots can be generated with the following code snippet for further analysis

```
net1.feature_visualization([net1.evol_weights],
sample_interval, intervals, plotx=5, ploty=6)
net1.animation([net1.evol_weights], plotx=5,
ploty=6, sample_interval=sample_interval,
intervals=intervals)
net1.spike_statistics()
```

The `net1.feature_visualization` method generates a plot given in Figure 5 and the method `net1.animation` generates an animation of evolved

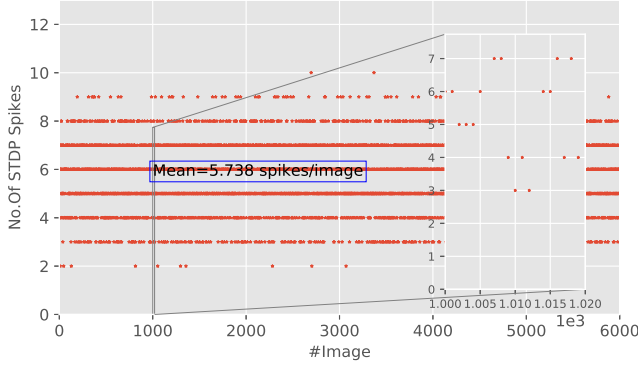


Fig. 19. Spikes per image in layer L2. Shown in the inset zoomed to show images 1000 to 1020.

features in Conv1⁵. The `net1.spike_statistics` method produces the plots shown in Figures 18 and 19. The first convolution layer (Conv1) was trained by passing 6000 EMNIST images through the network. Figure 18 shows the number of times each of the 30 maps had their weights updated as the 6000 training images passed through the network. The number of STDP spikes (weight updates) for each of the 6000 training images are shown in Figure 19. For example, images 1000 and 1001 (see inset) each had 6 STDP spikes meaning that 6 of the 30 maps of L2 had their weights updated as these images went through the network.

2) Stopping criteria:

$$C_l \triangleq \frac{\sum_{w,k,i,j} (W_l(w,k,i,j) * (1 - W_l(w,k,i,j)))}{n_l} \quad (22)$$

W_l are the weights (synapses) of l^{th} layer, specifically, for the first convolution layer with 30 maps, $W_{l=2}(w,k,i,j) \in \mathbb{R}^{30 \times 2 \times 5 \times 5}$ with $n_{l=2} = 30 \times 2 \times 5 \times 5 = 1500$, and for the second convolution layer with 200 maps, $W_{l=4}(w,k,i,j) \in \mathbb{R}^{200 \times 30 \times 5 \times 5}$ with $n_{l=4} = 200 \times 30 \times 5 \times 5 = 150000$. Kheradpisheh et al [31] defined a convergence factor given in Equation (22) to stop the training if $0.01 < C_l < 0.02$. If the elements in W_l all approach either 0 or 1 then $C_l \rightarrow 0$. This stopping criteria indicates the weights are near saturation and no additional weight updates will then matter. In this work, during training, the weights (synapses) are sampled after every 200 images (see Figure 23) have passed through the network. In the initial phases of the training, the weights (synapses) approach 0.5 because, as Figure 23 indicates, the value of C_l approaches 0.2 (See ⁶). Another way to determine if the network is finished learning is to look at the temporal difference of the weights (synapses) as defined by Equation (23). The corresponding plot for our experiment is shown in Figure 24.

Temporal Difference \triangleq

$$\frac{\sum_{w,k,i,j} (W_l^{[t-1]}(w,k,i,j) - W_l^{[t]}(w,k,i,j))^2}{n_l} \quad (23)$$

⁵<https://www.youtube.com/watch?v=KA4IJe2AtvE>

⁶The weights in feature extraction layers are bounded between 0 and 1. The maximum of $w(1-w)$ is at $w = 0.25$. C_l is the average of these values for all the weights and $C_l = 0.25$ if and only if all the weights equal 0.5.

3) *Collecting spikes in Pool 1 (with and without lateral inhibition)*: Once the first convolutional layer (L2) is trained, the weights of L2 (Conv1) are fixed and input spikes from L1 are simply passed through L2 and pooled in L3 (Pool 1). Lateral inhibition is still applied as the spikes pass through L2 so that only the dominant feature map will be allowed to produce spike. However, STDP competition is *not* applied because there is no training involved as the L2 weights are now fixed. There is also an option to enforce or not to enforce lateral inhibition in L3 (Pool 1) layer. In the following code snippet, setting `pool_lateral_inh=False` results in lateral inhibition in L3 (Pool 1) being turned off. Setting `pool_spike_accum=False` (as done in this work) restricts the number of spikes per neuron in L3 to at most one. Below code snippet collects spikes in Pool 1 *without* lateral inhibition.

```
evolved_weights = net1.evol_weights[-1]
#First Pool and Conv layers, note that train=False
net2 = network.Network(output_channels=30,\
pool_lateral_inh=False, inputs=train_input_images,\
train=False, set_weights=evolved_weights,\
debug=False, save_pool_spike_tensor=True,\
threshold=15.0, save_pool_features=True,\
pool_spike_accum=False)
net2.rewire_weights() # fixing the weights
net2.feedforward()
fig = net2.spikes_per_map_per_class(plot_x=1,
plot_y=2, class_labels=class_labels_train,\
pool_output_data=net2.pool_spike_tensor,\
labels_map=labels_map, view_maps=[25, 30],\
final_weights=evolved_weights,\
labels_map=labels_dict)
```

If `pool_lateral_inh` is set to True then lateral inhibition is turned on in the pooling layer. (As shown in Figure 20, this case results in lesser spikes per map per label compared to that of Figure 6.) Below code snippet collects spikes in Pool 1 *with* lateral inhibition.

```
evolved_weights = net1.evol_weights[-1]
#First Pool and Conv layers, note that train=False
net3 = network.Network(output_channels=30,\
pool_lateral_inh=True, inputs=train_input_images,\
train=False, set_weights=evolved_weights,\
debug=False, save_pool_spike_tensor=True,\
threshold=15.0, save_pool_features=True,\
pool_spike_accum=False)
net3.rewire_weights() # fixing the weights
net3.feedforward()
fig = net2.spikes_per_map_per_class(plot_x=1,
plot_y=2, class_labels=class_labels_train,\
pool_output_data=net2.pool_spike_tensor,\
labels_map=labels_map, view_maps=[25, 30],\
final_weights=evolved_weights,\
labels_map=labels_dict)
```

4) *Feature classification in Pool 1*: The `net2.spikes_per_map_per_class` method was used to produce Figure 6. This figure shows only two of 30 maps in layers L2 and L3 as `view_maps=[25, 30]`. The spikes for each image are collected in layer L3 as a tensor giving $S_{L3}(t) \in \mathbb{R}^{12 \times 30 \times 11 \times 11}$. 12 is the number of time steps per image, 30 is the number of maps in L2/L3, and 11×11 is the shape of each map in L3 (pooling layer). This spike tensor is summed over the 12 time steps giving $S_{L3}^{total} \triangleq \sum_{t=0}^{11} S_{L3}(t) \in \mathbb{R}^{30 \times 11 \times 11}$. S_{L3}^{total}

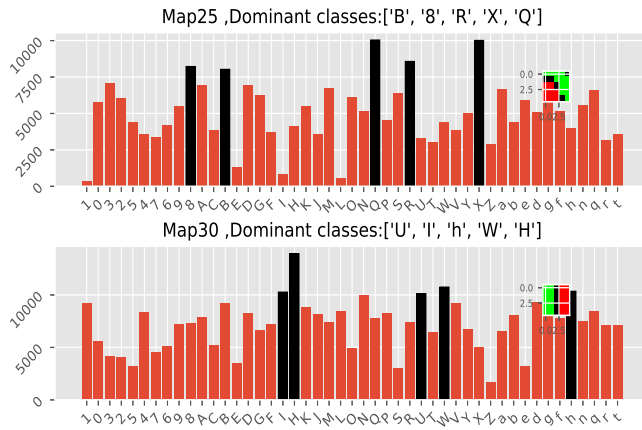


Fig. 20. Spikes per map per label. Highlighted (in black) are the classes that resulted in most number of spikes in a particular feature map. Features learned by a map are shown in the inset. Notice that the number of spikes in general is less compared to Figure 6.

is then flattened to obtain a binary spike feature vector in \mathbb{R}^{3630} ($30 \times 11 \times 11 = 3630$). Note that the keyword `save_pool_features` in the object `net2` must be set to `True` in order to create spike feature vectors. Generated spike features are classified using an ANN provided in `classifierclass.py` as shown in the below code snippet. However, in this work we used ANNs with binary activations and surrogate gradients to classify the spike feature vectors.

```
train_pool_spike_features = net2.make_feature_vecs\
(net2.pool_spike_features)
n_classes = 47
n_hidden = 1
net_struct = \
[train_pool1_spike_features.shape[1],1500,n_classes]
log_path = 'path'
#path to log data to be visualized in tensorboard
neural_net = cls.Classifier(train_data=\
(train_pool1_spike_features, class_labels_train),\
test_data=(test_pool1_spike_features,\
class_labels_test), network_structure=net_struct,\
activation_fns=activation_fns, epochs=10, eta=0.001,\
lmbda=0.0001, verbose=1, plots=True,\
optimizer='adam', eta_decay_factor=1.007,\
patience=8, eta_drop_type='plateau', epochs_drop=1,\
val_frac=0.091, drop_out=0.0, ip_lyr_drop_out=0.0,\
leaky_alpha=0.1, leaky_relu=False,\
weight_init='he_uniform', bias_init=0.1,\
batch_size=5, log_path=log_path)
neural_net.keras_fcn_classifier()
```

B. Conv2 and Pool 2 without lateral inhibition in Pool 1

If a second convolution layer is added to the network, the accumulated spikes in L3 (Pool 1 with or without lateral inhibitions) can be used as input to train this second convolution layer (Conv2) as shown below. Using the spikes collected from L3 (Pool 1) without lateral inhibition the code for this 2nd convolution layer is as follows:

```
nTrain_images = 35000, 14_maps = 200
#35k are enough if lateral inh in pool1 is False
size = net2.pool_spike_tensor.shape[0]
input_channels = net2.pool_spike_tensor.shape[2]
inputs = \
```

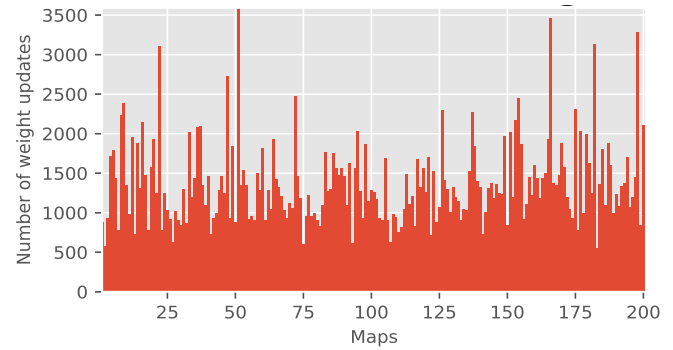


Fig. 21. Number of spikes that resulted in STDP weight updates per map in Conv2.

```
net2.pool_spike_tensor[:, :, 0:nTrain_images*tsteps]
net4 = network.Network(pool_lateral_inh=False,\
inputs=inputs, A_plus=0.0002, debug=False,\
output_channels=14_maps, size=size,\
input_channels=input_channels, lr_inc_rate=1500,\
sample_interval=200, train=True,\
threshold=15.0, inh_reg=3, epochs=1)
net4.feedforward()
```

1) *Generating plots:* Various plots for Conv2 (Pool 2) can be generated with the following code for further analysis

```
layer_num = [2, 3, 4] #conv1, pool1, pool2
filter_sizes = [net2.conv_kernel_size,\
net3.pool_kernel_size, net4.conv_kernel_size]
filter_strides = [1, 2, 1]
nof_filters = [net2.output_channels,\
net3.output_channels, net4.output_channels]
#[list of #filters from first conv to last layers]
types = ['conv', 'pool', 'conv']
layer_weights=[net2.evol_weights],\
[net4.evol_weights]], currLayer= 4
#[list of synapses from first conv to last conv]
fig = net4.feature_visualization(layer_weights,\
sample_interval, intervals, plotx=5, ploty=5,\
layer_num=layer_num, filter_sizes=filter_sizes,\
nof_filters=nof_filters, types=types,\
currLayer=currLayer, show=True)
net4.feature_convergence([net1.evol_weights, \
net4.evol_weights], sample_interval)
animation, fig = net4.animation(layer_weights,\
sample_interval, intervals, plotx=10, ploty=10,\
layer_num=layer_num, filter_sizes=filter_sizes,\
filter_strides=filter_strides, currLayer=currLayer,\
types=types, nof_filters=nof_filters)
```

The `net4.feature_convergence` method was used to generate plots shown in Figures 23 and 24 and these plots show that the synapses of the Conv2 layer converge slower than layer L2 (Conv1). Such behavior is expected as the Conv2 layer tries to learn features that are more complex than that of the features in layer L2 (Conv1). For a Conv2 layer trained with spikes collected without lateral inhibition in layer L3 (Pool 1) an early stopping mechanism based on the temporal differences can be used (see [35]) and an example plot is shown in Figure 24). The `net4.spike_statistics()` method was used to generate plots shown in Figure 21 and Figure 22.

The `net4.animation()` method is used to produce an animation of Conv2 features⁷. Spikes were collected in Pool 2 layer by fixing the weights of layer L4 (Conv1). The spikes

⁷<https://www.youtube.com/watch?v=xtywjRcHmaI>

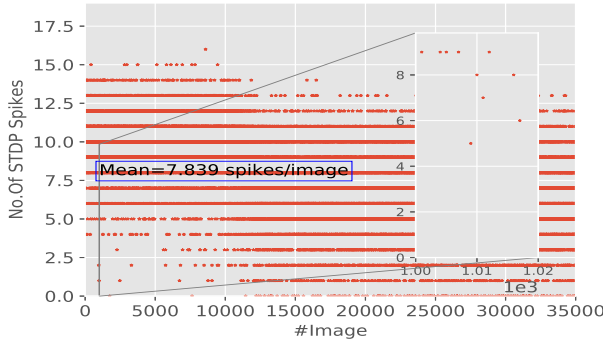


Fig. 22. Spikes per image in Conv2. Shown in the inset zoomed to show images 1000 to 1020.

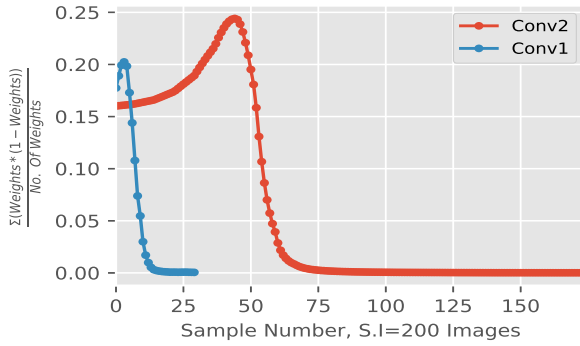


Fig. 23. Convergence plots for layers L2 (Conv1) and Conv2.

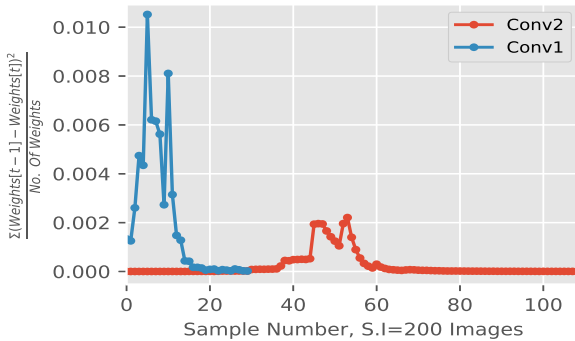


Fig. 24. Temporal difference plots for layers L2 (Conv1) and Conv2.

per map per label in Pool 2 layer are shown in Figure 25 similar to layer L3 (Pool 1). The accumulated spikes in Pool 2 can be converted into spike feature vectors using the method `network.make_feature_vecs()` with the resulting feature vectors classified using the class `inputlayerclass`.

The `net4.feature_visualization()` method was used to generate the plots of some of the features of the Conv2 layer as shown in Figure 26.

C. Conv2 and Pool 2 with lateral inhibition in Pool 1

The synapses in L4 (Conv2) are also trained using the spikes collected in L3 (Pool 1) with lateral inhibition.

```
nTrain_images = 60000, 14_maps = 200
#conv2 needs more training if lateral inh in\
#pool1 is False
```

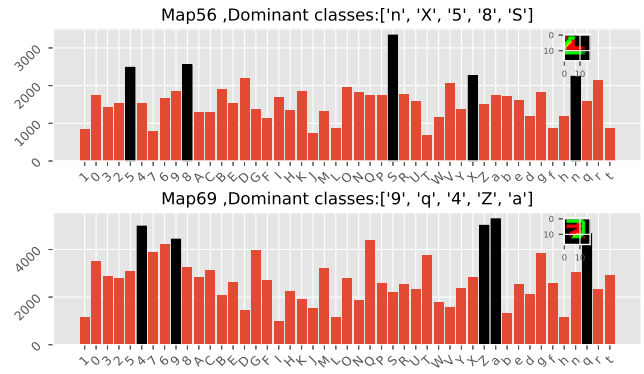


Fig. 25. Spikes per map per label in Pool 2. Highlighted (in black) are the classes that resulted in most number of spikes in a particular feature map. Feature learned by a map is shown in the inset.

```
size = net3.pool_spike_tensor.shape[0]
input_channels = net3.pool_spike_tensor.shape[2]
inputs = \
net3.pool_spike_tensor[:, :, 0:nTrain_images*tsteps]
net5 = network.Network(pool_lateral_inh=False, \
inputs=inputs, A_plus=0.0002, debug=False, \
output_channels=14_maps, size=size, \
input_channels=input_channels, lr_inc_rate=1500, \
sample_interval=200, train=True, \
threshold=15.0, inh_reg=3, epochs=2)
net5.feedforward()
```

Convergence plots for the weights in the Conv2 layer (with inhibition in pool 1) are shown in Figure 27 and Figure 28

Spike statistics for the Conv2 layer are given in Figure 29 and Figure 30.

The weights (synapses) at the end of the training of Conv2 are given in Figure 31. The animation of the feature evolution for the Conv2 weights is given at ⁸.

Similar to spikes per map per label in layer L3 (Pool 1), a similar plot for L5 (Pool 2) is also generated and is shown in Figure 32. As the spikes are already accumulated in L5 (Pool 2), they are converted into spike feature vectors using the method `make_feature_vecs` as described for layer L3 (Pool 1).

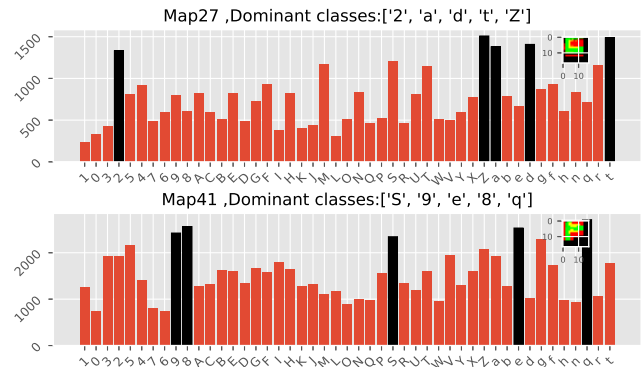


Fig. 32. Spikes per map per label in L5. Highlighted (in black) are the classes that resulted in the most number of spikes in a particular feature map. Feature learned by a map is shown in the inset.

⁸<https://www.youtube.com/watch?v=rL51343G-Yk&t=24s>

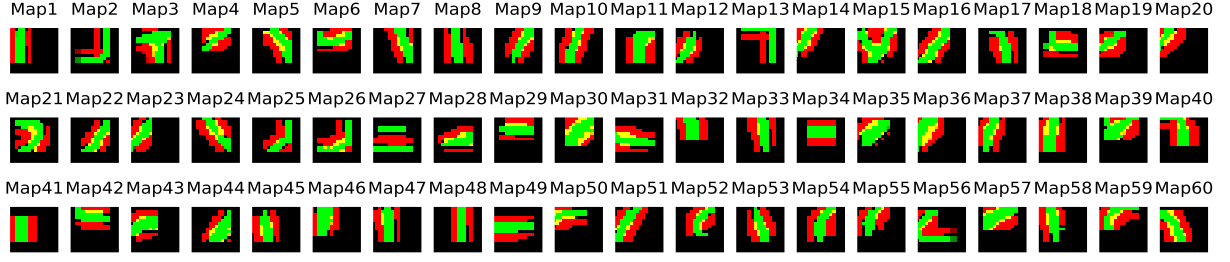


Fig. 26. Evolved features in L4 (Conv2).

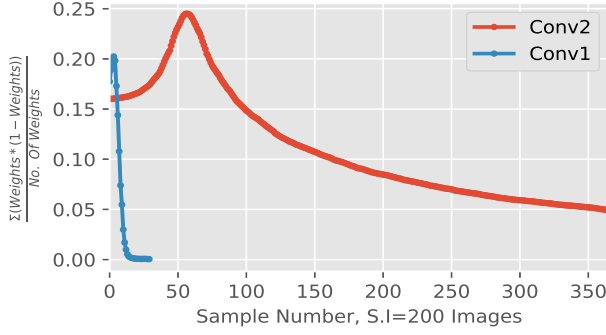


Fig. 27. Temporal difference plot for Conv2 synapses when trained with spikes collected from L3 layer (Pool 1) with lateral inhibition.

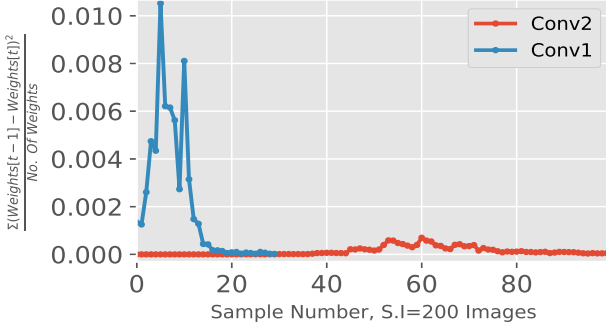


Fig. 28. Temporal difference plot for Conv2 synapses when trained with spikes collected from L3 layer (Pool 1) with lateral inhibition.

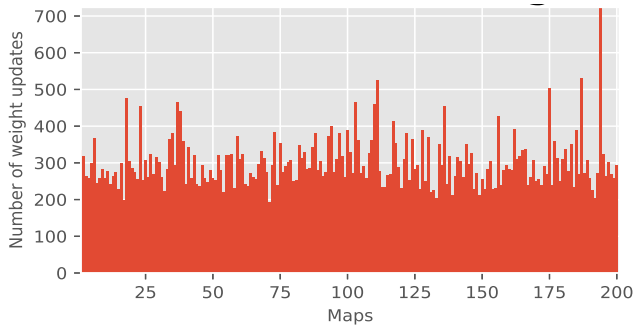


Fig. 29. Number of spikes that resulted in STDP weight updates per map.

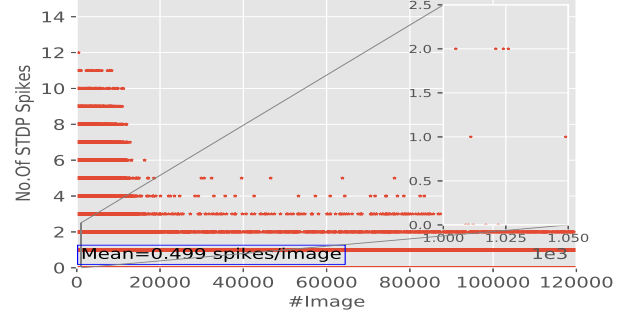


Fig. 30. Spikes per image in layer L4. Notice that mean spikes per image is up to $10\times$ lesser than the case where layer L4 (Conv2) was trained without lateral inhibition in layer L3 (Pool 1).

VIII. CONCLUSIONS

We have shown that by combining biologically inspired methods (latency encoded spikes, STDP) and backpropagation (with surrogate gradients) one can achieve up to 85.3% accuracy with the EMNIST dataset. This was done using backpropagation only in the classification layers of the network as the classification layers are decoupled from the feature extraction layers. The accuracy achieved here is quite comparable to the 85.57% accuracy reported in [48] which used rate encoded (Poisson) input spikes in a network with one hidden layer of 800 neurons and with backpropagation performed in all the layers. We also demonstrated an accuracy of 94.5% when the classifier was given the information that an input image was a letter (upper or lower case) or a digit. As discussed in the paper, this conditioning was considered because of the indistinguishability of some of the data between some of the classes (e.g., {0,O} in Figure 10).

Using a conventional deep convolution network Shawon et al [49] report an accuracy of 90.59% on the balanced EMNIST (see also the survey paper [50]). The deep network in [49] consisted of 6 convolution layers, a hidden layer with 64 neurons followed by a classification layer.

The computational advantages of using binary activations with respect to a custom hardware implementation [51] [38] [39] [52] [53] [54] of bio-inspired neural networks were also presented. The software tool SPYKEFLOW was developed and used to simulate the network and visualize its results. The SPYKEFLOW tool provides useful information to the users about feature extraction and spike activity at various stages

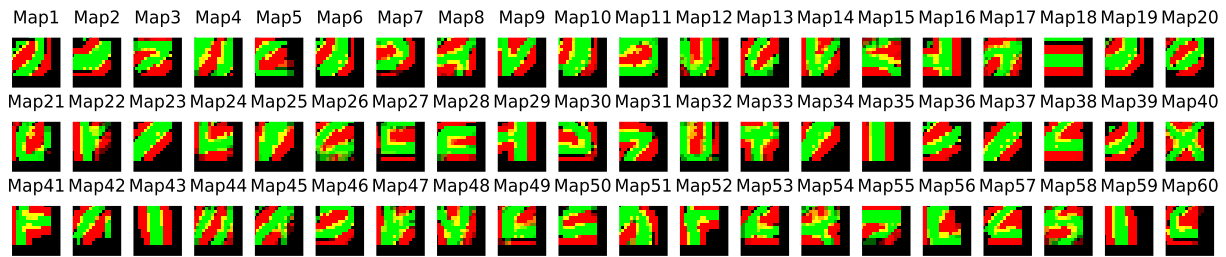


Fig. 31. Final synapses of L4 layer (Conv2) at the end of training. Notice that the evolved features are more complex when compared to those in Figure 26.

of the spiking network serving as a diagnostic tool of learning in SNNs.

IX. ACKNOWLEDGMENTS

Ruthvik Vaila is thankful to the Electrical and Computer Engineering Department, Boise State University, Idaho, USA for providing him a graduate assistantship (GA) to carry out this work.

REFERENCES

- [1] A. Delorme, L. Perrinet, and S. J. Thorpe, "Networks of integrate-and-fire neurons using Rank Order Coding B: Spike timing dependent plasticity and emergence of orientation selectivity," *Neurocomputing*, vol. 38-40, pp. 539 – 545, 2001, computational Neuroscience: Trends in Research 2001. [Online]. Available: <http://www.sciencedirect.com/science/article/pii/S0925231201004039>
- [2] M. Kiselev, "Rate coding vs. temporal coding - is optimum between?" in *2016 International Joint Conference on Neural Networks (IJCNN)*, July 2016, pp. 1355–1359.
- [3] H. Markram, W. Gerstner, and P. J. Sjöström, "Spike-Timing-Dependent Plasticity: A Comprehensive Overview," *Frontiers in Synaptic Neuroscience*, vol. 4, p. 2, 2012. [Online]. Available: <https://www.frontiersin.org/article/10.3389/fnsyn.2012.00002>
- [4] T. Masquelier, R. Guyonneau, and S. J. Thorpe, "Spike Timing Dependent Plasticity Finds the Start of Repeating Patterns in Continuous Spike Trains," *PLOS ONE*, vol. 3, no. 1, pp. 1–9, 01 2008. [Online]. Available: <https://doi.org/10.1371/journal.pone.0001377>
- [5] L. Bottou, F. E. Curtis, and J. Nocedal, "Optimization Methods for Large-Scale Machine Learning," 2016.
- [6] Y. Lecun, L. Bottou, Y. Bengio, and P. Haffner, "Gradient-based learning applied to document recognition," *Proceedings of the IEEE*, vol. 86, no. 11, pp. 2278–2324, Nov 1998.
- [7] C. Frenkel, M. Lefebvre, and D. Bol, "Learning without feedback: Direct random target projection as a feedback-alignment algorithm with layerwise feedforward training," 2019.
- [8] J. C. R. Whittington and R. Bogacz, "Theories of Error Back-Propagation in the Brain," *Trends in Cognitive Sciences*, vol. 23, no. 3, pp. 235–250, Jan. 2020. [Online]. Available: <https://doi.org/10.1016/j.tics.2018.12.005>
- [9] S. Grossberg, "Competitive learning: From interactive activation to adaptive resonance," *Cognitive Science*, vol. 11, no. 1, pp. 23 – 63, 1987. [Online]. Available: <http://www.sciencedirect.com/science/article/pii/S0364021387800253>
- [10] Q. Liao, J. Z. Leibo, and T. Poggio, "How Important is Weight Symmetry in Backpropagation?" *arXiv e-prints*, p. arXiv:1510.05067, Oct 2015.
- [11] A. Rocke, *The weight transport problem*. paulispace, Jun 2017. [Online]. Available: <https://paulispace.com/deep/learning/2017/06/30/weight-transport.html>
- [12] T. Lillicrap, D. Cownden, D. Tweed, and C. J. Akerman, "Random synaptic feedback weights support error backpropagation for deep learning," *Nature Communications*, vol. 7, p. 13276, 11 2016.
- [13] E. O. Neftci, C. Augustine, S. Paul, and G. Detorakis, "Event-Driven Random Back-Propagation: Enabling Neuromorphic Deep Learning Machines," *Frontiers in Neuroscience*, vol. 11, p. 324, 2017. [Online]. Available: <https://www.frontiersin.org/article/10.3389/fnins.2017.00324>
- [14] Y. LeCun, C. Cortes, and C. Burges, "Mnist handwritten digit database," *ATT Labs [Online]*. Available: <http://yann.lecun.com/exdb/mnist>, vol. 2, 2010.
- [15] A. Krizhevsky, V. Nair, and G. Hinton, "The CIFAR-10 dataset," May 2012. [Online]. Available: <https://www.cs.toronto.edu/~kriz/cifar.html>
- [16] M. Courbariaux, I. Hubara, D. Soudry, R. El-Yaniv, and Y. Bengio, "Binarized Neural Networks: Training Deep Neural Networks with Weights and Activations Constrained to +1 or -1," 2016.
- [17] C. Lee, P. Panda, G. Srinivasan, and K. Roy, "Training Deep Spiking Convolutional Neural Networks With STDP-Based Unsupervised Pre-training Followed by Supervised Fine-Tuning," *Frontiers in Neuroscience*, vol. 12, p. 435, 08 2018.
- [18] J. Deng, W. Dong, R. Socher, L.-J. Li, K. Li, and L. Fei-Fei, "ImageNet: A Large-Scale Hierarchical Image Database," 2009.
- [19] N. Anwani and B. Rajendran, "NormAD - Normalized Approximate Descent based supervised learning rule for spiking neurons," in *2015 International Joint Conference on Neural Networks (IJCNN)*, July 2015, pp. 1–8.
- [20] J. H. Lee, T. Delbruck, and M. Pfeiffer, "Training Deep Spiking Neural Networks Using Backpropagation," *Frontiers in Neuroscience*, vol. 10, p. 508, 2016. [Online]. Available: <https://www.frontiersin.org/article/10.3389/fnins.2016.00508>
- [21] A. Tavanaei, Z. Kirby, and A. Maida, "Training Spiking ConvNets by STDP and Gradient Descent," *2018 International Joint Conference on Neural Networks (IJCNN)*, pp. 1–8, 07 2018.
- [22] J. C. Thiele, O. Bichler, A. Dupret, S. Solinas, and G. Indiveri, "A Spiking Network for Inference of Relations Trained with Neuromorphic Backpropagation," p. arXiv:1903.04341, Mar 2019.
- [23] B. Rueckauer, I.-A. Lungu, Y. Hu, and M. Pfeiffer, "Theory and Tools for the Conversion of Analog to Spiking Convolutional Neural Networks," *arXiv e-prints*, p. arXiv:1612.04052, Dec 2016.
- [24] T. Masquelier, "Spike-based computing and learning in brains, machines, and visual systems in particular (hdr report)," Ph.D. dissertation, Université Toulouse III - Paul Sabatier, 10 2017.
- [25] I. M. Comsa, K. Potempa, L. Versari, T. Fischbacher, A. Gesmundo, and J. Alakuijala, "Temporal coding in spiking neural networks with alpha synaptic function," *arXiv e-prints*, p. arXiv:1907.13223, Jul 2019.
- [26] B. Gardner and A. Grüning, "Supervised Learning in Spiking Neural Networks for Precise Temporal Encoding," *PLOS ONE*, vol. 11, no. 8, pp. 1–28, 08 2016. [Online]. Available: <https://doi.org/10.1371/journal.pone.0161335>
- [27] S. R. Kheradpisheh and T. Masquelier, "S4nn: temporal backpropagation for spiking neural networks with one spike per neuron," 2019.
- [28] H. Mostafa, "Supervised Learning Based on Temporal Coding in Spiking Neural Networks," *IEEE Transactions on Neural Networks and Learning Systems*, vol. 29, no. 7, pp. 3227–3235, July 2018.
- [29] P. Panda, A. Aketi, and K. Roy, "Towards Scalable, Efficient and Accurate Deep Spiking Neural Networks with Backward Residual Connections, Stochastic Softmax and Hybridization," 2019.
- [30] S. R. Kheradpisheh, M. Ganjtabesh, S. J. Thorpe, and T. Masquelier, "STDP-based spiking deep convolutional neural networks for object recognition," *Neural Networks*, vol. 99, pp. 56 – 67, 2018. [Online]. Available: <http://www.sciencedirect.com/science/article/pii/S0893608017302903>
- [31] S. R. Kheradpisheh, M. Ganjtabesh, and T. Masquelier, "Bio-inspired unsupervised learning of visual features leads to robust invariant object recognition," *Neurocomputing*, vol. 205, pp. 382 – 392, 2016. [Online]. Available: <http://www.sciencedirect.com/science/article/pii/S0925231216302880>
- [32] S. R. Kheradpisheh, private communication.

- [33] J. Conradt, R. Berner, M. Cook, and T. Delbruck, "An embedded AER dynamic vision sensor for low-latency pole balancing," in *2009 IEEE 12th International Conference on Computer Vision Workshops, ICCV Workshops*, Sep. 2009, pp. 780–785.
- [34] R. Vaila, J. Chiasson, and V. Saxena, "Deep Convolutional Spiking Neural Networks for Image Classification," *arXiv e-prints*, p. arXiv:1903.12272, Mar 2019.
- [35] R. Vaila, J. Chiasson, and V. Saxena, "Feature Extraction Using Spiking Convolutional Neural Networks," in *Proceedings of the International Conference on Neuromorphic Systems*, ser. ICONS 19. New York, NY, USA: Association for Computing Machinery, 2019. [Online]. Available: <https://doi.org/10.1145/3354265.3354279>
- [36] M. A. Nielsen, *Neural Networks and Deep Learning*. Determination Press, Jan 2015. [Online]. Available: <http://neuralnetworksanddeeplearning.com/>
- [37] G. Cohen, S. Afshar, J. Tapson, and A. van Schaik, "EMNIST: an extension of MNIST to handwritten letters," *arXiv e-prints*, p. arXiv:1702.05373, Feb. 2017.
- [38] X. Wu, V. Saxena, and K. Zhu, "Homogeneous Spiking Neuromorphic System for Real-World Pattern Recognition," *IEEE Journal on Emerging and Selected Topics in Circuits and Systems*, vol. 5, no. 2, pp. 254–266, June 2015.
- [39] X. Wu, V. Saxena, K. Zhu, and S. Balagopal, "A CMOS Spiking Neuron for Brain-Inspired Neural Networks With Resistive Synapses and In Situ Learning," *IEEE Transactions on Circuits and Systems II: Express Briefs*, vol. 62, no. 11, pp. 1088–1092, Nov 2015.
- [40] V. S. Ruthvik Vaila, John Chiasson, "Spiking CNNs with PYNN and NEURON," in *NICE Workshop Series*. Portland, Oregon, USA: Intel, Feb. 2019. [Online]. Available: https://www.researchgate.net/publication/335635588_Spiking_CNNs_with_PYNN_and_NEURON
- [41] M. Hines and T. Carnevale, *NEURON Simulation Environment*. New York, NY: Springer New York, 2013, pp. 1–8, In Encyclopedia of Computational Neuroscience, Jaeger, Dieter and Jung, Ranu, Editors. [Online]. Available: https://doi.org/10.1007/978-1-4614-7320-6_795-1
- [42] T. Bekolay, J. Bergstra, E. Hunsberger, T. DeWolf, T. Stewart, D. Rasmussen, X. Choo, A. Voelker, and C. Eliasmith, "Nengo: a Python tool for building large-scale functional brain models," *Frontiers in Neuroinformatics*, vol. 7, p. 48, 2014. [Online]. Available: <https://www.frontiersin.org/article/10.3389/fninf.2013.00048>
- [43] M. Mozafari, M. Ganjtabesh, A. Nowzari-Dalini, and T. Masquelier, "SpykeTorch: Efficient Simulation of Convolutional Spiking Neural Networks With at Most One Spike per Neuron," *Frontiers in Neuroscience*, vol. 13, p. 625, 2019. [Online]. Available: <https://www.frontiersin.org/article/10.3389/fnins.2019.00625>
- [44] A. Paszke, S. Gross, F. Massa, A. Lerer, J. Bradbury, G. Chanan, T. Killeen, Z. Lin, N. Gimelshein, L. Antiga, A. Desmaison, A. Kopf, E. Yang, Z. DeVito, M. Raison, A. Tejani, S. Chilamkurthy, B. Steiner, L. Fang, J. Bai, and S. Chintala, "PyTorch: An Imperative Style, High-Performance Deep Learning Library," in *Advances in Neural Information Processing Systems 32*, H. Wallach, H. Larochelle, A. Beygelzimer, F. d'Alché Buc, E. Fox, and R. Garnett, Eds. Curran Associates, Inc., 2019, pp. 8024–8035. [Online]. Available: <http://papers.neurips.cc/paper/9015-pytorch-an-imperative-style-high-performance-deep-learning-library.pdf>
- [45] S. v. d. Walt, S. C. Colbert, and G. Varoquaux, "The NumPy Array: A Structure for Efficient Numerical Computation," *Computing in Science & Engineering*, vol. 13, no. 2, pp. 22–30, 2011. [Online]. Available: <https://aip.scitation.org/doi/abs/10.1109/MCSE.2011.37>
- [46] M. Abadi, A. Agarwal, P. Barham, E. Brevdo, Z. Chen, C. Citro, G. S. Corrado, A. Davis, J. Dean, M. Devin, S. Ghemawat, I. Goodfellow, A. Harp, G. Irving, M. Isard, Y. Jia, R. Jozefowicz, L. Kaiser, M. Kudlur, J. Levenberg, D. Mané, R. Monga, S. Moore, D. Murray, C. Olah, M. Schuster, J. Shlens, B. Steiner, I. Sutskever, K. Talwar, P. Tucker, V. Vanhoucke, V. Vasudevan, F. Viégas, O. Vinyals, P. Warden, M. Wattenberg, M. Wicke, Y. Yu, and X. Zheng, "TensorFlow: Large-Scale Machine Learning on Heterogeneous Systems," 2015, software available from tensorflow.org. [Online]. Available: <https://www.tensorflow.org/>
- [47] J. D. Hunter, "Matplotlib: A 2D graphics environment," *Computing in Science & Engineering*, vol. 9, no. 3, pp. 90–95, 2007.
- [48] Y. Jin, P. Li, and W. Zhang, "Hybrid Macro/Micro Level Backpropagation for Training Deep Spiking Neural Networks," *arXiv e-prints*, 05 2018.
- [49] A. Shawon, M. Jamil-Ur Rahman, F. Mahmud, and M. M. Arefin Zaman, "Bangla handwritten digit recognition using deep cnn for large and unbiased dataset," in *2018 International Conference on Bangla Speech and Language Processing (ICBSLP)*, Sep. 2018, pp. 1–6.
- [50] A. Baldominos, Y. Saez, and P. Isasi, "A Survey of Handwritten Character Recognition with MNIST and EMNIST," *Applied Sciences*, vol. 9, no. 15, 2019. [Online]. Available: <https://www.mdpi.com/2076-3417/9/15/3169>
- [51] V. Saxena, X. Wu, I. Srivastava, and K. Zhu, "Towards Neuromorphic Learning Machines Using Emerging Memory Devices with Brain-Like Energy Efficiency," *Journal of Low Power Electronics and Applications*, vol. 8, no. 4, 2018. [Online]. Available: <http://www.mdpi.com/2079-9268/8/4/34>
- [52] X. Wu and V. Saxena, "Dendritic-Inspired Processing Enables Bio-Plausible STDP in Compound Binary Synapses," *IEEE Transactions on Nanotechnology*, vol. PP, 01 2018.
- [53] R. C. Ivans, S. G. Dahl, and K. D. Cantley, "A Model for R(t) Elements and R(t)-Based Spike-Timing-Dependent Plasticity With Basic Circuit Examples," *IEEE Transactions on Neural Networks and Learning Systems*, pp. 1–11, 2019.
- [54] S. G. Dahl, R. Ivans, and K. D. Cantley, "Modeling Memristor Radiation Interaction Events and the Effect on Neuromorphic Learning Circuits," in *Proceedings of the International Conference on Neuromorphic Systems*, ser. ICONS '18. New York, NY, USA: ACM, 2018, pp. 1:1–1:8. [Online]. Available: <http://doi.acm.org/10.1145/3229884.3229885>